Published in final edited form as:
Neuroscience. 2008 December 2; 157(3): 606–620. doi:10.1016/j.neuroscience.2008.09.020.

Progressive synaptic pathology of motor cortical neurons in a BAC transgenic mouse model of Huntington's Disease

Jay Spampanato, PhD[1], **Xiaofeng Gu, MD, PhD**[2], **X. William Yang, MD, PhD**[2,*], and **Istvan Mody, PhD**[1]

[1] Department of Neurology, David Geffen School of Medicine, University of California, Los Angeles, California 90095, USA

[2] Center for Neurobehavioral Genetics, Semel Institute for Neuroscience and Human Behavior, Department of Psychiatry & Biobehavioral Sciences, Brain Research Institute, University of California, Los Angeles, California 90095, USA

Abstract

Huntington's disease (HD) is a neurodegenerative disorder caused by a polyglutamine repeat expansion in huntingtin. A newly developed BAC transgenic mouse model (BACHD) reproduces phenotypic features of HD including predominantly neuropil associated protein aggregation and progressive motor dysfunction with selective neurodegeneration. Motor dysfunction has been shown to precede neuropathology in BACHD mice. We therefore investigated the progression of synaptic pathology in pyramidal cells and interneurons of the superficial motor cortex of BACHD mice. Whole-cell patch clamp recordings were performed on layer 2/3 primary motor cortical pyramidal cells and PV interneurons from BACHD mice at 3 months, when the mice begin to demonstrate mild motor dysfunction, and at 6 months, when the motor dysfunction is more severe. Changes in synaptic variances were detectable at 3 months and at 6 months BACHD mice display progressive synaptic pathology in the form of reduced cortical excitation and loss of inhibition onto pyramidal cells. These results suggest that progressive alterations of the superficial cortical circuitry may contribute to the decline of motor function in BACHD mice. The synaptic pathology occurs prior to neuronal degeneration and may therefore prove useful as a target for future therapeutic design.

Keywords

Pyramidal cell; interneuron; huntingtin; degeneration; parvalbumin; inhibition

Huntington's Disease (HD) is an autosomal dominant neurodegenerative disorder resulting from a mutant huntingtin (htt) gene that contains a CAG (glutamine) repeat expansion beyond 36 at its N-terminal coding region. Huntingtin normally contains a cassette of less than 34 consecutive glutamines. Age of onset and disease severity are inversely correlated to the magnitude of the CAG repeat expansion such that HD patients present with symptoms from 2

*Co-Corresponding Authors: Istvan Mody, Ph.D., UCLA Neurology, NRB1 Rm. 575D, 635 Charles E. Young Drive South, Los Angeles, CA 90095-7335, Ph: 310-206-4481, Fax: 310-825-0033, E-mail: mody@ucla.edu, X. William Yang. M.D.. Ph.D., UCLA Psychr & Biobehav Sci, Center for Neurobehavioral Genetics, Semel Institute, David Geffen School of Medicine at UCLA, BOX 951761, 3309 Gonda, Los Angeles, CA 90095-1761, Ph: 310-267-2761, E-mail: xwyang@mednet.ucla.edu.
Section Editor: (Molecular Neuroscience): Dr. Werner Sieghart, Brain Research Institute, University of Vienna, Division of Biochemistry and Molecular Biology, Spitalgasse 4, A-1090 Vienna, Austria

years to 80 years of cognitive impairments and progressive motor dysfunction such as bradykinesia and chorea (The Huntington's Disease Collaborative Research Group, 1993; Andrew et al., 1993; Brinkman et al., 1997; Vonsattel and DiFiglia, 1998). Though mutant htt is ubiquitously expressed throughout the body and the CNS (Strong et al., 1993), neuropathology of HD brains shows specific striatal and cortical degeneration marked by a loss of medium spiny neurons (MSN) and pyramidal cells, respectively (Vonsattel and DiFiglia, 1998); however, early diagnosis and animal models of HD have suggested that synaptic pathology precedes motor dysfunction (Vonsattel et al., 1985; Levine et al., 2004; Reading et al., 2004; Paulsen et al., 2006; Cepeda et al., 2007; Aylward, 2007).

A newly developed HD mouse model (BACHD) was generated by microinjection of a modified BAC containing the full length human htt genomic DNA with 97 mixed CAA-CAG repeats (Gray et al., 2008). The BACHD mice demonstrate anatomical and physiological similarities consistent with adult onset HD and display motor deficits on the Rotarod test as early as 2 months of age that progressively decline by 6 and 12 months. Motor dysfunction occurs earlier than detectable neuropathological changes: striatal and cortical volume loss, protein aggregation and neuronal degeneration beyond 12 months (Gray et al., 2008). This model adds further evidence in support of the hypothesis that the progression of motor dysfunction in HD results from functional changes in the corticostriatal circuitry that precede significant neuronal atrophy in either region (Laforet et al., 2001; Cepeda et al., 2003; Li et al., 2003b; Starling et al., 2005; Andre et al., 2006; Milnerwood and Raymond, 2007). In contrast to an enormous wealth of research into the molecular, cellular and physiological changes associated with HD the critical early functional changes that precede the onset of motor dysfunction and neurodegeneration are still unknown (Cepeda et al., 2007).

Initial electrophysiological analysis of MSNs of 6 month old BACHD mice demonstrated a selective reduction of large amplitude (>20 pA) spontaneous excitatory post-synaptic currents (sEPSC) with no changes in passive membrane properties or action potential firing (Gray et al., 2008). This selective difference combined with the lack of pathological degeneration of striatal neurons suggests a possible role of cortical dysfunction in the progression of motor dysfunction in BACHD mice. Analysis of an independent animal model of HD has previously demonstrated a specific deficit of spontaneous inhibitory post-synaptic currents (sIPSC) onto superficial cortical pyramidal cells (Gu et al., 2005). To investigate the cortical circuitry of BACHD mice they were first crossed with G42 mice which were shown to express green-fluorescent protein (GFP) in a subset of parvalbumin (PV) interneurons in the cortex (Chattopadhyaya et al., 2004). PV interneurons were specifically investigated because they account for approximately 50% of the total number of cortical interneurons and are known to be a critical component of synchronized neuronal activity (Gonchar and Burkhalter, 1997; Klausberger et al., 2003; Hajos et al., 2004; Gu et al., 2005; Fuchs et al., 2007).

Experimental Procedures

Breeding and Genotyping

All surgical, sampling protocols were approved by UCLA Chancellor's Animal Research Committee and are in accordance with the *Guide for the Care and Use of Laboratory Animals* by the National Institutes of Health. Animals were maintained in climate-controlled housing with a 12 h light/dark cycle and were given food and water *ad libitum.* BACHD mice were generated and maintained on an FvB/NJ background. G42 mice were originally generated on C57BL/6 background (Chattopadhyaya et al., 2004) and backcrossed onto the FvB/NJ for 10 generations. Breeding pairs consisted of 2 female heterozygous BACHD mice and 1 male heterozygous G42 mouse per cage. Genotyping was done as previously described (Chattopadhyaya et al., 2004; Gray et al., 2008). BACHD +/− and G42 +/− double transgenic mice as well as their BACHD −/− and G42 +/− littermates were used for the recordings.

Slice Preparation

Coronal slices were cut from 3 or 6 month old BACHD or BACHDxG42 mice and WT or WTxG42 littermates; a total of 31 animals. Brains were quickly removed and placed into ice-cold normal artificial cerebrospinal fluid (aCSF) containing (in mM): 126 NaCl, 2.5 KCl, 2 $CaCl_2$, 2 $MgCl_2$, 1.25 $NaHPO_4$, 26 $NaHCO_3$, 10 D-Glucose, 1.5 Glutamine, 1.5 Na-Pyruvate with pH 7.3–7.4 when bubbled with 95% O_2-5% CO_2. Normal aCSF was supplemented with 3 mM kynurenic acid (Sigma-Aldrich, St. Louis, MO) for the duration of the cutting procedure. 350 μm thick slices containing primary motor cortex and/or striatum were cut in the coronal orientation using a Leica VT1000S Vibratome, (Leica Microsystems, Wetzlar, Germany). The slices were then transferred to an interface style holding chamber containing normal aCSF aerated with 95% O_2 and 5% CO_2 at 32°C and allowed to recover for at least one hour prior to experimentation.

Electrophysiology

Slices were placed in a submerged recording chamber modified to promote laminar flow and perfused at >8 ml/min with an extracellular recording solution containing (in mM): 126 NaCl, 2.5 KCl, 2 $CaCl_2$, 2 $MgCl_2$, 1.25 $NaHPO_4$, 26 $NaHCO_3$, 10 D-Glucose, 1.5 Glutamine, 1.5 Na-Pyruvate. The recording solution was aerated with 95% O_2 and 5% CO_2 and the bath temperature was maintained at 33–34°C. Microelectrodes (3–6 MΩ when filled) were pulled from 7740 glass (Garner Glass Company, Claremont, CA) and filled with an internal recording solution containing (in mM): 140 Cs-Methane Sulfonate, 5 NaCl, 10 HEPES, 0.2 EGTA, 2 Mg-ATP, 0.2 Na-GTP and 5 QX-314 (pH=7.3, 280–290 mOsmol). Whole-cell recordings were performed in voltage clamp mode on visually identified primary motor cortex layer 2/3 pyramidal cells and GFP containing PV interneurons of the same region. In most cases both sEPSC and sIPSC were recorded in the same cell by first holding at the reversal potential for sIPSC (−60 mV) and then depolarizing and holding at the reversal potential for sEPSC (+20 mV). Under these recording conditions the Nernst equation predicts a reversal potential for sIPSC of −60 mV and a reversal potential for sEPSC of 0 mV. The recording potential of +20 mV for sEPSC in our experiments was empirically determined by first depolarizing the cells to the predicted Nernst potential and then gradually increasing the holding potential to more positive voltages until sEPSC were no longer detectable. The more positive than predicted reversal for sEPSC is likely due to the difficulty in space clamping the extended dendrites (where excitatory synapses are found) complicated by the high frequency of synaptic activity in our tissue. The accuracy of our empirical determination of sEPSC reversal potential was confirmed in *post-hoc* analysis of decay kinetics. As sEPSC decay is much faster than sIPSC decay, a contamination of our sIPSC recordings by sEPSC would have produced a population of events with much faster kinetics, which was not observed in our recordings. Whole cell capacitance and series resistance were monitored and recordings were made with >70% series resistance compensation using the Axon Instruments MultiClamp 700A or Axopatch 200B (Molecular Devices Corp., Sunnyvale, CA) at 10 kHz sampling frequency through a 3 kHz low pass filter with EVAN data collection software (LabVIEW-based in house software). Recordings were terminated if the series resistance exceeded 25 MΩ. Events were detected from 30 to 60 s of raw data low pass filtered at 1 kHz (Bessel). Events smaller in amplitude than three times the baseline standard deviation (approximately 3–5 pA after low pass filtered) were eliminated prior to analysis. Frequencies, amplitudes and rise-times were measured from the batched data typically containing more than one thousand events. Kinetics of decay were measured by fitting the unitary averaged traces from isolated single events with an exponential function. sEPSC onto PV interneurons were best fit with a double exponential, however even with extensive attempts to eliminate overlapping events due to the high frequency of activity in these cells the τ_{slow} component was considered to be an inaccurate representation of the kinetics of channel inactivation and was therefore discarded. In each case the average ratio of current inactivated with the τ_{fast} component was greater than 80% and was therefore considered

to be a more accurate measure. Passive membrane properties were measured in response to a sequential 5 mV square pulse which was averaged over multiple trials to eliminate contamination of active ongoing synaptic activity. Non-stationary noise analysis was conducted using the EVAN analysis software as previously described (De Koninck and Mody, 1994; Dalby and Mody, 2003).

For a more global analysis of synaptic activity that eliminates the complications of detecting single events we also calculated the I-Mean for each cell as previously reported (Glykys and Mody, 2007). In brief, I-Mean is calculated by averaging the value of all the digitized points of a given epoch (1 s) that fall outside the baseline Gaussian noise. This calculation was performed for each second of data and then averaged to produce the I-Mean for each cell, typically during a period of two to three minutes. This measure is sensitive to subtle compounded changes in amplitude, frequency and kinetics of synaptic activity and has been shown to be capable of detecting the combined changes in all three properties that may have been considered insignificant when analyzed individually (Glykys and Mody, 2007). All values for I-mean are reported as mean ± standard deviation.

Statistical significance was determined using the Student's t-test function in Microsoft Excel. The F-test was first used to determine if the variance of the data set differed significantly between WT and BACHD in each individual comparison. An F-test of $p \leq 0.05$ was considered significant. When the variance of the data was significantly different a heteroscedastic t-test was performed on that data. In all other cases a homoscedastic t-test was performed. Means were considered significantly different at $p \leq 0.05$ and values of $p \leq 0.01$ and are indicated as such.

Experiments were performed blind to genotype which was revealed only after data analyses were completed. Tail samples were kept for *post-hoc* genotype confirmation. When calculating cumulative probabilities for groups of cells that differed by more than one cell, events in the larger group were randomized and the number of events was reduced to match the size of the smaller group.

Results

3 Month Old BACHD Mice

The neuroanatomy and pathology of BACHD mice are described extensively by Gray *et. al* (Gray et al., 2008). In summary, BACHD mice exhibit selective cortical and striatal atrophy and mutant htt aggregation patterns reminiscent of adult-onset HD. The progressive motor deficit is detectable at 2 months of age and becomes robust by 6 months. However, at this time the animals lack a detectable cellular pathology in either the cortex or the striatum. This model provides an excellent opportunity to identify the functional changes in neuronal circuitry that correlate with motor dysfunction but precede the onset of HD-like neuropathology in a full length mutant human htt mouse model.

We performed whole-cell patch clamp recordings from pyramidal cells and PV interneurons of layer 2/3 primary motor cortex from 3 month old BACHD and G42 (BACHDxG42) double transgenic animals and wild-type G42 (WTxG42) littermates. G42 mice express GFP in a subset (~50%) of cortical PV interneurons allowing for *a priori* identification of these cells (Chattopadhyaya et al., 2004). We observed a similar quantity and distribution of GFP cells between BACHDxG42 and WTxG42 mice in both 3 month and 6 month old animals that was consistent with the original description of G42 mice (Chattopadhyaya et al., 2004) and the laminar pattern of PV expression reported for the motor cortex (Porter et al., 2000). In all cases, recordings were performed in the absence of any pharmacological blockers to specifically allow for the residual network excitation and inhibition to remain intact while both types of

synaptic activity were independently measured from each cell. Under these conditions the majority of the recorded events are action potential independent miniature synaptic currents. This was confirmed by recording in the presence of 1 μM TTX and 50 μM $CdCl_2$ to block action potential dependent activity. With action potentials blocked we observed a similar ~30% reduction of synaptic activity in each cell type and both genotypes (data not shown).

Cortical pyramidal cells are known to degenerate in post-symptomatic HD and a reduced inhibition on to superficial cortical pyramidal cells has been reported in transgenic mice expressing mutant htt exon 1 (Gu et al., 2005). We therefore began by recording sEPSC and sIPSC in pyramidal cells of layer 2/3 primary motor cortex to determine if reduced pyramidal cell inhibition is a common phenotype of animal models of HD. To address the possibility of a progressive synaptic pathology we first recorded from 3 month old animals; an age at which the BACHD mice begin to perform worse than WT on the Rotarod test (Gray et al., 2008).

In 3 month old animals we were unable to identify any significant differences in either the frequency, amplitude, 10–90% rise-time or decay of sIPSC or sEPSC measured in cortical pyramidal cells from BACHD mice compared to wild-type littermates (Fig 1A, Fig 2). The means were remarkably similar and there were no significant differences in the variances in either of the data sets (Table 1). It is not surprising from these data that we also observed a similar I-Mean for sIPSC (WT: 5.35 ± 2.54 pA, BACHD: 5.62 ± 3.58 pA) and sEPSC (WT: 1.16 ± 0.33 pA, BACHD: 0.99 ± 0.61 pA) for motor cortical layer 2/3 pyramidal cells (Table 1).

Likewise there were no significant differences in mean frequency, amplitude, 10–90% rise-time or decay of sIPSC or sEPSC recorded in PV interneurons from the same region (Fig 1B, Fig 2). For PV interneurons there were however significantly smaller variances in the decay rates of both sEPSC and sIPSC in the BACHD mice ($p \leq 0.05$, F-test). Again however, these data produced a similar I-Mean for sIPSC (WT: 2.15 ± 2.22 pA, BACHD: 1.89 ± 1.76 pA) and sEPSC (WT: 1.32 ± 0.40 pA, BACHD: 1.60 ± 0.74 pA) in motor cortical layer 2/3 PV interneurons (Table 1). However the I-Mean sEPSC variance was significantly larger for BACHD PV interneurons ($p \leq 0.05$, F-test).

Since this region of the cortex was observed to be normal at this age and the MSN of the striatum were observed to have a selective deficit of large amplitude sEPSC at 6 months (Gray et al., 2008), we recorded from MSN in 3 month old mice. Again, there were no significant differences in the mean data for either sIPSC or sEPSC onto MSN from BACHD mice compared to wild-type littermates at 3 months (Fig 1C, Fig 2). Despite identical mean sEPSC 10–90% rise-times for MSN from the two genotypes the data from the BACHD mice had a significantly smaller variance ($p \leq 0.05$, F-test), though the opposite was true for the sIPSC amplitudes (Table 1). These data also resulted in no significant differences in the I-Mean for sIPSC (WT: 4.04 ± 1.27 pA, BACHD: 2.94 ± 1.07 pA) and sEPSC (WT: 1.02 ± 0.23 pA, BACHD: 0.78 ± 0.44 pA) in striatal MSN (Table 1). However the I-Mean sEPSC variance was significantly larger for BACHD MSN ($p \leq 0.05$, F-test).

The similarities between both genotypes for each cell type can be seen in the single cell comparisons of the raw data and normalized average unitary current overlays in Figure 1. These individual cell comparisons were representative of the group data for all pyramidal cells, PV interneurons and MSNs recorded from 3 month old animals (Fig 2). The averaged data (mean ± standard deviation) for each cell type is presented in Table 1. All three cell types also exhibited similar membrane mean input resistances and time-constants when compared within groups between BACHD mice and wild-type littermates (Table 1). However both the MSN and PV interneurons from BACHD mice had significantly more variable membrane time-constants than those from WT mice ($p \leq 0.05$, F-test).

These data indicate that the observed subtle motor dysfunction in 2 month old BACHD mice is either the result of changes that are below the detection level of our electrophysiological experiments (Williams and Mitchell, 2008) or take place in an entirely different cell type or circuit. Though, we cannot rule out the possibility that the observed changes in the variances of the data sets may play some role in the developing motor dysfunction of the BACHD animals (Aradi and Soltesz, 2002; Santhakumar and Soltesz, 2004; Aradi et al., 2004).

6 Month Old BACHD Mice

The motor deficit of BACHD mice becomes very robust by 6 months of age. Due to the progressive severity of the motor dysfunction at this age, the selective change reported in MSNs at 6 months (Gray et al., 2008), and the implication of cortical inhibition in a different mouse model of HD (Gu et al., 2005) we investigated the possibility that the BACHD mice would have more robust functional changes in cortical circuitry manifest as either larger variances or significant differences in mean synaptic activity.

Whole cell patch clamp recordings from layer 2/3 primary motor cortex revealed a significant reduction in the frequency of sIPSC onto pyramidal cells of 6 month old BACHD mice compared to wild-type littermates (Fig 3). Figure 3 illustrates that the reduction in the frequency of sIPSC recorded in a typical pyramidal cell of a 6 month old BACHD animal is noticeable at the level of the raw trace comparison (Fig 3A). The averaged unitary trace overlay shows that while the frequency was reduced, there was no change in either the amplitude or the kinetics of the sIPSC. The cumulative probability and histogram plots of more than 2,600 sequential events from two pyramidal cells further illustrate the shift towards longer inter-event intervals with no change in the amplitude of sIPSC in the cortex of the BACHD mice (Fig 3B, C). The grouped data demonstrate on average a 17% reduction in the frequency of sIPSC onto cortical pyramidal cells of BACHD mice ($p \leq 0.01$, Student's t-Test) with no difference in either the amplitude or the kinetics of these events (Fig 3D, Table 2). The cumulative probability across all cells (>8,000 events) further illustrates the consistent and significant shift of the mean towards longer inter-event intervals with no change in the amplitude of sIPSC in BACHD mice (Fig 3E). The I-Mean and variance for inhibition on to layer 2/3 pyramidal cells of the primary motor cortex of BACHD mice was also significantly smaller than WT (WT: 10.62 ± 6.02 pA, BACHD: 7.34 ± 3.29 pA; $p \leq 0.05$, Student's t-Test; $p \leq 0.05$, F-test; Table 2). Finally, when pyramidal sIPSC I-Mean was compared within genotypes we found that WT pyramidal cell sIPSC I-Mean increased significantly in both mean and variance from 3 month to 6 month old animals ($p \leq 0.01$, Student's t-Test; $p \leq 0.05$, F-test) while BACHD pyramidal cell sIPSC I-Mean did not (Table 1, Table 2). The I-Mean increase can be attributed in part to a 26% increase in sIPSC frequency onto WT pyramidal cells from 3 to 6 months compared to a smaller 14% increase in the BACHD mice during the same period.

When sEPSC were recorded in cortical pyramidal cells from BACHD mice there were no immediately obvious differences compared to wild-type littermates. Figure 4 illustrates the single cell comparison of raw traces as well as the overlay of the average unitary sEPSC from those two cells (Fig 4A). Cumulative probability and event histograms of more than 2,400 events from each cell show similar amplitude and inter-event interval probabilities (Fig 4B, C). Finally, the grouped data from all recordings demonstrated no significant changes in the mean or variances of the frequency, amplitude, 10–90% rise-time and decay time of sEPSC in cortical pyramidal cells from BACHD mice and wild-type littermates (Fig 4D). The group averages are displayed in Table 2 as well as the passive membrane properties which were also not significantly different. Though the changes in the isolated sEPSCs were not significant the combined I-Mean analysis resulted in a significantly smaller excitation on to pyramidal cells from BACHD mice (WT: 1.38 ± 0.54 pA, BACHD: 0.75 ± 0.30 pA; $p \leq 0.01$, Student's t-Test; Table 2). The significant reduction in I-Mean was produced by the combined, but individually

non-significant 12% reductions in sEPSC frequency and amplitude in the pyramidal cells of the BACHD mice compared to WT. BACHD mice also had a significantly smaller variance of sEPSC I-Mean at 6 months old compared to 3 month old BACHD pyramidal cells ($p \leq 0.05$, F-test; Table 1, 2).

The specific deficit of cortical pyramidal cell inhibition in the BACHD mice extends our earlier findings in a mutant htt fragment model of HD (Gu et al., 2005) to a full length mutant htt mouse model, thus strengthening the hypothesis that alterations in cortical inhibition contribute to the functional deficits in HD, and are not just an anomaly of the previous animal model. Because of the nature of the intra- and interlaminar cortical connectivity one of the primary candidates for a reciprocal or homeostatic change is PV interneurons which account for 50% of all neocortical interneurons (Gonchar and Burkhalter, 1997; Porter et al., 2000; Thomson and Bannister, 2003; Bannister, 2005). We therefore further investigated the possibility that PV interneurons also display a synaptic pathology correlated with the progressive severity of motor dysfunction in BACHD mice at 6 months.

In contrast to the pyramidal cells, raw trace comparisons and trace overlays of the average unitary IPSC between 6 month old BACHD mice and wild-type littermates recorded from PV interneurons of layer 2/3 primary motor cortex showed no obvious differences (Fig 5A). The amplitude and frequency cumulative probability plots and event histograms of more than 2,200 sIPSC from each cell confirmed no detectable differences between PV interneurons from the two genotypes (Fig 5B, C). Grouped data and averages of all recordings demonstrate the similarities observed between BACHD mice and wild-type littermates for the mean and variance of the frequency, amplitude, 10–90% rise-time and decay time of sIPSC (Fig 5D, Table 2). As expected from the aforementioned similarities there was no difference in the I-Mean of inhibition onto the PV interneurons between WT and BACHD mice (WT: 3.63 ± 2.07 pA, BACHD: 4.02 ± 2.28 pA; Table 2).

In contrast to pyramidal cells, raw trace comparisons and average unitary current overlays of sEPSC onto PV interneurons in BACHD mice revealed a significant reduction ($p \leq 0.01$, Student's t-Test) in both frequency and amplitude and a significantly slower ($p \leq 0.05$, Student's t-Test) 10–90% rise-time (Fig 6A, Table 2). The comparison of over 2,100 events from these two representative cells illustrates a shift in the cumulative probability and event distribution of sEPSC amplitudes towards smaller events in the BACHD mice as well as a shift in the inter-event intervals towards longer durations (Fig 6B, C). This trend was consistent for the grouped data and averages which demonstrate both a 30% reduction in the frequency and 18% reduction in the amplitude of sEPSC onto PV interneurons of BACHD mice while the kinetics of those events remain unchanged (Fig 6D, Table 2). The cumulative probability of 7,000 combined events from all cells demonstrates that the overall reduction in excitatory synaptic drive onto PV interneurons of BACHD mice manifests as an increase in the probability of smaller events over the entire range of amplitudes as well as a shift in the inter-event interval towards longer periods (Fig 6E). Not surprisingly, these significant reductions in the mean frequency and mean amplitude combine to produce a significant reduction in the I-Mean and variance of excitation onto PV interneurons of BACHD mice compared to WT (WT: 1.72 ± 0.90 pA, BACHD: 0.92 ± 0.44 pA; $p \leq 0.01$, Student's t-Test; $p \leq 0.05$, F-test; Table 2). Furthermore, BACHD mice exhibit a significant loss of excitation onto PV interneurons in the form of reduced sEPSC amplitude and I-Mean from 3 months to 6 months ($p \leq 0.01$, Student's t-Test), while WT mice exhibit an increase in sEPSC frequency and I-Mean variance during the same period ($p \leq 0.05$, Student's t-Test; $p \leq 0.05$, F-test; Table 1, 2).

The reduction in amplitude of sEPSC on to parvalbumin interneurons in BACHD mice could result from changes in the presynaptic release machinery or from post synaptic changes in receptor number or channel conductance. Because the synaptic changes we observed appear

to be cell specific and may be the result of local circuitry changes, it would be difficult to accurately test this hypothesis using traditional evoked release experiments. We therefore performed a non-stationary noise analysis (NSNA) on the spontaneous events to determine if there might be a detectable global change in the spontaneous excitatory activity on to parvalbumin interneurons in BACHD mice. For accurate determination of single channel conductances, large amplitude, presumably action potential evoked synaptic events were eliminated and the remaining events were narrowed to a small population of uncontaminated single synaptic events (50–100 per cell) with a complete decay to baseline. Figure 7 illustrates the raw traces from one WT and one BACHD parvalbumin interneuron with the average overlaid (Fig 7A), example plots demonstrating the three conductance states present in the WT and two in the BACHD mice (Fig 7B), as well as histograms of the combined data from each genotype (Fig 7C). Consistent with previously published data demonstrating single channel conductance states of AMPA-R (Derkach et al., 1999) the WT PV interneuron histogram was fit with a triple Gaussian corresponding to cell average excitatory synaptic conductances of 12.0 pS, 24.1 pS, and 36.6 pS. In contrast, the BACHD histogram was best fit with a double Gaussian corresponding only to conductances of 12.1 pS and 23.9 pS. These data suggest that the reduced excitation onto PV interneurons in BACHD mice can be attributed to a failed post-synaptic mechanism resulting in cells with excitatory synapses remaining in lower conductance states.

Discussion

BACHD mice express full length human mutant htt and reproduce several key behavioral and pathological features reminiscent of those found in HD patients. However, mutant htt aggregation and selective cortical and striatal atrophy, two HD-like pathological phenotypes in BACHD mice, are found to follow evidence of neuronal dysfunction in this and other animal models of HD (Levine et al., 2004; Cepeda et al., 2007; Gray et al., 2008). Motor dysfunction in BACHD mice is progressive with minor deficits occurring at 2 months followed by more severe deficits at 6 and 12 months (Gray et al., 2008). This model provides an excellent opportunity to investigate, in a full length human mutant htt expressing animal, the earliest detectable functional changes occurring in the corticostriatal circuitry, which is postulated to be critical to selective neuropathogenesis in HD (Vonsattel et al., 1985; Levine et al., 2004; Cepeda et al., 2007). Unlike previous electrophysiological studies of other mouse models addressing cognitive deficits associated with HD (Usdin et al., 1999; Murphy et al., 2000; Lynch et al., 2007), we focused our study on the motor deficits that define the disorder using a top-down approach, beginning in the pattern generating, superficial layers of the primary motor cortex which has been previously implicated in a truncation model of HD (Gu et al., 2005).

Our data show that even though BACHD mice have motor deficits at 2 months old they have no detectable changes in mean excitation or inhibition onto layer 2/3 cortical pyramidal cells, PV interneurons or striatal MSNs at 3 months old. At this time only variance changes in synaptic activity are detectable. These results suggest that the corticostriatal circuit may develop normally in young adult BACHD mice, and provide the first electrophysiological evidence that the deficits in cortical function are truly progressive in a full length mutant htt mouse model. We detected the first functional changes at 6 months postnatal in the form of a specific reduction in inhibition onto cortical pyramidal cells and a reduction in excitation onto both PV interneurons and pyramidal cells of the same region. This occurs at a time when MSNs are reported to have a selective reduction in large amplitude (>20 pA) sEPSC (Gray et al., 2008) suggesting that functional deficits in the cortical circuitry occur concomitant with changes in the striatum in BACHD brains (for review of the extensive literature regarding changes in MSNs and the striatum in HD see (Cepeda et al., 2007)).

The lack of significant differences at 3 months in the mean synaptic activity onto the three cell types tested does not immediately exclude the possibility that these cells function abnormally and contribute to the physiological phenotype of motor dysfunction. Computational modeling and dynamic-clamp studies in *in vitro* slice preparations have demonstrated that a significant change in the variance of a single synaptic property with no concomitant change in the mean is sufficient to produce major changes in action potential firing rates and neuronal synchronization (Aradi and Soltesz, 2002; Santhakumar and Soltesz, 2004; Aradi et al., 2004). At 3 months, when the motor deficit is minor, there are significant changes in the variance of the kinetics of decay of both sIPSC and sEPSC in PV interneurons and the amplitude of sIPSC and kinetics of activation of sEPSC in MSN of BACHD mice. These same cell types also exhibit a significant increase in the variance of mean excitatory current in the BACHD mice. Variance changes indicate at the very least that these cells are likely to behave differently than their WT counterparts during complex network activity and can be interpreted as changes occurring at the molecular level in these cells at this time.

The data presented here suggest a progressive role of the local cortical circuitry (i.e., the superficial cortical layers) in the pathogenesis of neuronal dysfunction in HD. At 6 months, the decreased PV interneuron excitation and decreased pyramidal cell inhibition is consistent with the longstanding hypothesis of increased cortical excitability in HD. This could in turn increase excitation onto layer 5 pyramidal cells and subsequently increase the overall excitatory output onto striatal MSNs. However, an alternate interpretation follows from the primary role of PV interneurons in neuronal synchronization (Bartos et al., 2007). Network synchronization is a critical component of proper function within and between cortical and subcortical areas of the CNS (Jones, 2001; Bruno and Sakmann, 2006; Womelsdorf and Fries, 2007). The synchrony is created by the activity of interneurons and particularly fast-spiking, perisomatic targeting PV interneurons (Klausberger et al., 2003; Hajos et al., 2004; Buzsaki and Draguhn, 2004; Mann et al., 2005; Fuchs et al., 2007; Bartos et al., 2007). Reducing the activation of glutamate receptors specifically in PV interneurons to reduce the synaptic drive onto this population of interneurons reduced network synchronization in the hippocampus and the weak synchrony was attributed to imprecise spike-timing of PV interneurons (Fuchs et al., 2007). Furthermore, the resulting irregular inhibitory drive produced an increase in the frequency of action potential firing in pyramidal cells during synchronized network activity (Fuchs et al., 2007). Though the primary motor cortex lacks a granular layer 4 (Castro-Alamancos and Connors, 1997; Shipp, 2005), in the somatosensory cortex fast-spiking PV interneurons provide a critical feedforward inhibition of thalamocortical inputs to layer 4 (Daw et al., 2007; Cruikshank et al., 2007). This circuit is reliant on a well developed fast and large EPSC from thalamic afferents onto PV interneurons which results in a highly precise window of opportunity for pyramidal cell firing (Daw et al., 2007; Cruikshank et al., 2007). The primary motor cortex receives excitation and feed-forward inhibition from the somatosensory cortex (Ghosh and Porter, 1988) however neither these nor the thalamocortical afferents are well characterized (Ghosh and Porter, 1988; Porter et al., 1990; Shipp, 2005). It is possible that due to the reduced excitation of PV interneurons (coupled with the local deficit of inhibition onto pyramidal cells) the BACHD mice have impaired thalamocortical and corticocortical inputs and a reduced synchronization of these structures that could subsequently desynchronize the deeper layers and alter the overall output onto MSNs. It remains to be seen whether the corticostriatal pathways require the same level of synchronization for signal transmission as the thalamocortical pathway *in vivo*(Bruno and Sakmann, 2006) and whether desynchronization within and between cortical layers would result in enhanced or decreased excitation of MSNs. Reduced synchronization between cortical areas has recently been reported in pre-symptomatic HD patients (Thiruvady et al., 2007) and progressive reduction of corticostriatal connectivity is one possible mechanism for striatal atrophy and worsening motor dysfunction in HD (Cepeda et al., 2007).

We observed similar kinetics of synaptic events as previously described for both pyramidal cells and PV interneurons (Geiger et al., 1997; Gu et al., 2005). The majority of the events presented here are minis, suggesting that the observed deficits are the result of a failure of a synaptic mechanism or synapse maintenance in BACHD mice. Both normal htt and mutant htt interact with a number of important pre and postsynaptic proteins involved in vesicle transport, endocytosis, exocytosis and synaptic structure (Li et al., 2003b; Borrell-Pages et al., 2006; Truant et al., 2006). Li *et. al.* have previously shown that axon terminals of advanced HD mice contain fewer synaptic vesicles than WT mice and mutant htt binds more tightly to synaptic vesicles than WT htt culminating in a global reduction of glutamate release *in vitro*(Li et al., 2003a). Our finding of reduced frequency of sEPSC in PV interneurons is consistent with these reports. However our data initially suggest a cell specific deficit of excitation onto PV interneurons rather than between cortical pyramidal cells when synaptic excitation is analyzed using an individual event detection method. When the more global I-Mean method (Glykys and Mody, 2007) is used there is a near 2-fold reduction of excitation onto both pyramidal cells and PV interneurons of layer 2/3 of the primary motor cortex of BACHD mice. Our data for reduced global excitation in cortical pyramidal cells and changes in AMPA mediated synaptic activity in cortical neurons are consistent with early changes observed in the R6/2 and YAC mouse models (Andre et al., 2006; Milnerwood and Raymond, 2007). It should also be noted that the apparent cell specificity of the sEPSC deficit may be an inaccurate conclusion based on the limitations of the whole-cell voltage clamp technique combined with the differences in morphology between pyramidal cells and interneurons (Williams and Mitchell, 2008).

It is difficult to ascertain whether the differences reported here result from changes in the local superficial cortical circuitry or from changes in the corticocortical or thalamocortical afferents targeting these cells. If the superficial synaptic architecture of the motor cortex bears some resemblance to that of the somatosensory cortex where both layer 2/3 pyramidal cells and PV interneurons receive excitatory thalamic afferents and dense reciprocal excitation (Markram et al., 2004; Bannister, 2005), then according to our data there may be a post-synaptic mechanism of synaptic maintenance that is differentially affected in HD between pyramidal cells and PV interneurons. Indeed the NSNA of sEPSC onto PV interneurons suggests that mutant htt disrupts a post-synaptic mechanism in these cells and that disruption results in a failure of the cells' ability to increase AMPA/Kainate receptor conductance to higher states. GluR1 containing AMPA receptors are known to change conductance states in response to phosphorylation by Ca^{2+}/calmodulin-kinase II (CaM-KII) (Derkach et al., 1999) and this mechanism may have some specificity to parvalbumin interneurons (Ba et al., 2006). CaM-KII expression itself has previously been shown to be reduced in other models of HD (Deckel et al., 2001; Deckel et al., 2002) and mutant htt is reported to interact with calmodulin and various other CaM-KII expression regulatory proteins (Bao et al., 1996; Luthi-Carter et al., 2000).

Another candidate mechanism takes into account the role of BDNF in the cortex and HD (Cepeda et al., 2004; Lynch et al., 2007). Six month old BACHD mice are reported to have significantly reduced levels of BDNF (Gray et al., 2008). BDNF loss is a common phenotype of mouse models of HD and has been linked to the loss of WT htt function (Zuccato and Cattaneo, 2007). In separate studies, PV interneurons in other regions of the CNS have been shown to specifically require BDNF for proper electrophysiological and anatomical maturation, such as extensive dendritic arborization and synapse maintenance (Gorski et al., 2003; Berghuis et al., 2006; Itami et al., 2007). Coritcal PV interneurons of BACHD mice seem to develop normally up to 3 months, with the exception of the observed changes in the variances at this time, however the reduced mean frequency and amplitude of sEPSC compared to WT at 6 months is consistent with a failure of synaptic maintenance in these cells. This is supported by the comparison within genotypes from 3 to 6 month old animals. While WT PV interneurons experience an increase in sEPSC frequency and I-Mean variance, BACHD PV interneurons

experience a decrease in sEPSC amplitude and mean excitation during this time period. The decrease in sEPSC frequency suggests that the BACHD PV interneurons fail to continue to acquire new excitatory synapses and may experience some loss of excitatory drive over this time.

In conclusion, in a mouse model of HD we have demonstrated specific synaptic changes that occur in pyramidal cells and PV interneurons that occur concomitant with progressive decline of motor function but precede cellular atrophy and protein aggregation. The progressive synaptic dysfunction resulting in reduced cortical excitation and reduced inhibition of layer 2/3 pyramidal cells occurs in unison with a reduction of excitation onto striatal MSNs (Gray et al., 2008) suggesting a participatory role for cortical circuit dysfunction in HD.

Acknowledgments

This study was supported by grant NS30549 from NIH/NINDS and the Coelho Endowment to I.M. and by a grant from the Hereditary Disease Foundation, and grants NS049501and NS047391 from NIH/NINDS to XWY. We would like to thank Z. Josh Huang (Cold Spring Harbor) for providing the G42 mice.

Abbreviations

HD	Huntington’s disease
htt	huntingtin
BACHD	BAC transgenic mouse model
MSN	medium spiny neurons
sEPSC	spontaneous excitatory post-synaptic currents
sIPSC	spontaneous inhibitory post-synaptic currents
GFP	green-fluorescent protein
PV	parvalbumin
aCSF	artificial cerebrospinal fluid

Reference List

Andre VM, Cepeda C, Venegas A, Gomez Y, Levine MS. Altered cortical glutamate receptor function in the R6/2 model of Huntington’s disease. J Neurophysiol 2006;95:2108–2119. [PubMed: 16381805]

Andrew SE, Goldberg YP, Kremer B, Telenius H, Theilmann J, Adam S, Starr E, Squitieri F, Lin B, Kalchman MA, Graham RK, Hayden MR. The relationship between trinucleotide (CAG) repeat length and clinical features of Huntington’s disease. Nat Genet 1993;4:398–403. [PubMed: 8401589]

Aradi I, Santhakumar V, Soltesz I. Impact of heterogeneous perisomatic IPSC populations on pyramidal cell firing rates. J Neurophysiol 2004;91:2849–2858. [PubMed: 15136604]

Aradi I, Soltesz I. Modulation of network behaviour by changes in variance in interneuronal properties. J Physiol 2002;538:227–251. [PubMed: 11773331]

Aylward E. Changes in MRI striatal volumes as a biomarker in preclinical Huntington’s Disease. Brain Res Bull 2007;72:152–158. [PubMed: 17352939]

Ba M, Kong M, Yang H, Ma G, Lu G, Chen S, Liu Z. Changes in subcellular distribution and phosphorylation of GluR1 in lesioned striatum of 6-hydroxydopamine-lesioned and l-dopa-treated rats. Neurochem Res 2006;31:1337–1347. [PubMed: 17053970]

Bannister AP. Inter- and intra-laminar connections of pyramidal cells in the neocortex. Neurosci Res 2005;53:95–103. [PubMed: 16054257]

Bao J, Sharp AH, Wagster MV, Becher M, Schilling G, Ross CA, Dawson VL, Dawson TM. Expansion of polyglutamine repeat in huntingtin leads to abnormal protein interactions involving calmodulin. Proc Natl Acad Sci U S A 1996;93:5037–5042. [PubMed: 8643525]

Bartos M, Vida I, Jonas P. Synaptic mechanisms of synchronized gamma oscillations in inhibitory interneuron networks. Nat Rev Neurosci 2007;8:45–56. [PubMed: 17180162]

Berghuis P, Agerman K, Dobszay MB, Minichiello L, Harkany T, Ernfors P. Brain-derived neurotrophic factor selectively regulates dendritogenesis of parvalbumin-containing interneurons in the main olfactory bulb through the PLCgamma pathway. J Neurobiol 2006;66:1437–1451. [PubMed: 17013928]

Borrell-Pages M, Zala D, Humbert S, Saudou F. Huntington's disease: from huntingtin function and dysfunction to therapeutic strategies. Cell Mol Life Sci 2006;63:2642–2660. [PubMed: 17041811]

Brinkman RR, Mezei MM, Theilmann J, Almqvist E, Hayden MR. The likelihood of being affected with Huntington Disease by a particular age, for a specific CAG size. American Journal of Human Genetics 1997;60:1202–1210. [PubMed: 9150168]

Bruno RM, Sakmann B. Cortex is driven by weak but synchronously active thalamocortical synapses. Science 2006;312:1622–1627. [PubMed: 16778049]

Buzsaki G, Draguhn A. Neuronal oscillations in cortical networks. Science 2004;304:1926–1929. [PubMed: 15218136]

Castro-Alamancos MA, Connors BW. Thalamocortical synapses. Prog Neurobiol 1997;51:581–606. [PubMed: 9175158]

Cepeda C, Hurst RS, Calvert CR, Hernandez-Echeagaray E, Nguyen OK, Jocoy E, Christian LJ, Ariano MA, Levine MS. Transient and progressive electrophysiological alterations in the corticostriatal pathway in a mouse model of Huntington's Disease. J Neurosci 2003;23:961–969. [PubMed: 12574425]

Cepeda C, Starling AJ, Wu N, Nguyen OK, Uzgil B, Soda T, Andre VM, Ariano MA, Levine MS. Increased GABAergic function in mouse models of Huntington's Disease: reversal by BDNF. J Neurosci Res 2004;78:855–867. [PubMed: 15505789]

Cepeda C, Wu N, Andre VM, Cummings DM, Levine MS. The corticostriatal pathway in Huntington's disease. Prog Neurobiol 2007;81:253–271. [PubMed: 17169479]

Chattopadhyaya B, Di CG, Higashiyama H, Knott GW, Kuhlman SJ, Welker E, Huang ZJ. Experience and activity-dependent maturation of perisomatic GABAergic innervation in primary visual cortex during a postnatal critical period. J Neurosci 2004;24:9598–9611. [PubMed: 15509747]

Cruikshank SJ, Lewis TJ, Connors BW. Synaptic basis for intense thalamocortical activation of feedforward inhibitory cells in neocortex. Nat Neurosci 2007;10:462–468. [PubMed: 17334362]

Dalby NO, Mody I. Activation of NMDA Receptors in Rat Dentate Gyrus Granule Cells by Spontaneous and Evoked Transmitter Release. J Neurophysiol 2003;90:786–797. Ref Type: Generic. [PubMed: 12904493]

Daw MI, Ashby MC, Isaac JT. Coordinated developmental recruitment of latent fast spiking interneurons in layer IV barrel cortex. Nat Neurosci 2007;10:453–461. [PubMed: 17351636]

De Koninck Y, Mody I. Noise analysis of miniature IPSCs in adult rat brain slices: properties and modulation of synaptic GABAA receptor channels. J Neurophysiol 1994;71(4):1318–1335. Ref Type: Generic. [PubMed: 8035217]

Deckel AW, Elder R, Fuhrer G. Biphasic developmental changes in Ca2+/calmodulin-dependent proteins in R6/2 Huntington's disease mice. Neuroreport 2002;13:707–711. [PubMed: 11973475]

Deckel AW, Gordinier A, Nuttal D, Tang V, Kuwada C, Freitas R, Gary KA. Reduced activity and protein expression of NOS in R6/2 HD transgenic mice: effects of L-NAME on symptom progression. Brain Res 2001;919:70–81. [PubMed: 11689164]

Derkach V, Barria A, Soderling TR. Ca2+/calmodulin-kinase II enhances channel conductance of alpha-amino-3-hydroxy-5-methyl-4-isoxazolepropionate type glutamate receptors. Proc Natl Acad Sci U S A 1999;96:3269–3274. [PubMed: 10077673]

Fuchs EC, Zivkovic AR, Cunningham MO, Middleton S, Lebeau FE, Bannerman DM, Rozov A, Whittington MA, Traub RD, Rawlins JN, Monyer H. Recruitment of parvalbumin-positive interneurons determines hippocampal function and associated behavior. Neuron 2007;53:591–604. [PubMed: 17296559]

Geiger JR, Lubke J, Roth A, Frotscher M, Jonas P. Submillisecond AMPA receptor-mediated signaling at a principal neuron-interneuron synapse. Neuron 1997;18:1009–1023. [PubMed: 9208867]

Ghosh S, Porter R. Corticocortical synaptic influences on morphologically identified pyramidal neurones in the motor cortex of the monkey. J Physiol 1988;400:617–629. [PubMed: 3418539]

Glykys J, Mody I. The main source of ambient GABA responsible for tonic inhibition in the mouse hippocampus. J Physiol 2007;582:1163–1178. [PubMed: 17525114]

Gonchar Y, Burkhalter A. Three distinct families of GABAergic neurons in rat visual cortex. Cereb Cortex 1997;7:347–358. [PubMed: 9177765]

Gorski JA, Zeiler SR, Tamowski S, Jones KR. Brain-derived neurotrophic factor is required for the maintenance of cortical dendrites. J Neurosci 2003;23:6856–6865. [PubMed: 12890780]

Gray M, Shirasaki DS, Cepeda C, Andre VM, Wilburn B, Lu X-H, Tao J, Yamazaki I, Li SH, Li XJ, Levine MS, Yang XW. Full Length Human Mutant Huntingtin with a Stable Polyglutamine Repeat Can Elicit Progressive and Selective Neuropathogenesis in BACHD Mice. J Neurosci 2008;28:6182–6195. [PubMed: 18550760]

Gu X, Li C, Wei W, Lo V, Gong S, Li SH, Iwasato T, Itohara S, Li XJ, Mody I, Heintz N, Yang XW. Pathological cell-cell interactions elicited by a neuropathogenic form of mutant Huntingtin contribute to cortical pathogenesis in HD mice. Neuron 2005;46:433–444. [PubMed: 15882643]

Hajos N, Palhalmi J, Mann EO, Nemeth B, Paulsen O, Freund TF. Spike timing of distinct types of GABAergic interneuron during hippocampal gamma oscillations in vitro. J Neurosci 2004;24:9127–9137. [PubMed: 15483131]

Itami C, Kimura F, Nakamura S. Brain-derived neurotrophic factor regulates the maturation of layer 4 fast-spiking cells after the second postnatal week in the developing barrel cortex. J Neurosci 2007;27:2241–2252. [PubMed: 17329421]

Jones EG. The thalamic matrix and thalamocortical synchrony. Trends Neurosci 2001;24:595–601. [PubMed: 11576674]

Klausberger T, Magill PJ, Marton LF, Roberts JD, Cobden PM, Buzsaki G, Somogyi P. Brain-state- and cell-type-specific firing of hippocampal interneurons in vivo. Nature 2003;421:844–848. [PubMed: 12594513]

Laforet GA, Sapp E, Chase K, McIntyre C, Boyce FM, Campbell M, Cadigan BA, Warzecki L, Tagle DA, Reddy PH, Cepeda C, Calvert CR, Jokel ES, Klapstein GJ, Ariano MA, Levine MS, DiFiglia M, Aronin N. Changes in cortical and striatal neurons predict behavioral and electrophysiological abnormalities in a transgenic murine model of Huntington's disease. J Neurosci 2001;21:9112–9123. [PubMed: 11717344]

Levine MS, Cepeda C, Hickey MA, Fleming SM, Chesselet MF. Genetic mouse models of Huntington's and Parkinson's diseases: illuminating but imperfect. Trends Neurosci 2004;27:691–697. [PubMed: 15474170]

Li H, Wyman T, Yu ZX, Li SH, Li XJ. Abnormal association of mutant huntingtin with synaptic vesicles inhibits glutamate release. Hum Mol Genet 2003a;12:2021–2030. [PubMed: 12913073]

Li JY, Plomann M, Brundin P. Huntington's disease: a synaptopathy? Trends Mol Med 2003b;9:414–420. [PubMed: 14557053]

Luthi-Carter R, Strand A, Peters NL, Solano SM, Hollingsworth ZR, Menon AS, Frey AS, Spektor BS, Penney EB, Schilling G, Ross CA, Borchelt DR, Tapscott SJ, Young AB, Cha JH, Olson JM. Decreased expression of striatal signaling genes in a mouse model of Huntington's disease. Hum Mol Genet 2000;9:1259–1271. [PubMed: 10814708]

Lynch G, Kramar EA, Rex CS, Jia Y, Chappas D, Gall CM, Simmons DA. Brain-derived neurotrophic factor restores synaptic plasticity in a knock-in mouse model of Huntington's disease. J Neurosci 2007;27:4424–4434. [PubMed: 17442827]

Mann EO, Suckling JM, Hajos N, Greenfield SA, Paulsen O. Perisomatic feedback inhibition underlies cholinergically induced fast network oscillations in the rat hippocampus in vitro. Neuron 2005;45:105–117. [PubMed: 15629706]

Markram H, Toledo-Rodriguez M, Wang Y, Gupta A, Silberberg G, Wu C. Interneurons of the neocortical inhibitory system. Nat Rev Neurosci 2004;5:793–807. [PubMed: 15378039]

Milnerwood AJ, Raymond LA. Corticostriatal synaptic function in mouse models of Huntington's disease: early effects of huntingtin repeat length and protein load. J Physiol 2007;585:817–831. [PubMed: 17947312]

Murphy KP, Carter RJ, Lione LA, Mangiarini L, Mahal A, Bates GP, Dunnett SB, Morton AJ. Abnormal synaptic plasticity and impaired spatial cognition in mice transgenic for exon 1 of the human Huntington's disease mutation. J Neurosci 2000;20:5115–5123. [PubMed: 10864968]

Paulsen JS, Hayden MR, Stout JC, Langbehn DR, Aylward E, Ross CA, Guttman M, Nance M, Kieburtz K, Oakes D, Shoulson I, Kayson E, Johnson S, Penziner E. the Predict-HD Investigators of the Huntington Study Group. Preparing for preventive clinical trials: The predict-HD study. Arch Neurol 2006;63:883–890. [PubMed: 16769871]

Porter LL, Matin D, Keller A. Characteristics of GABAergic neurons and their synaptic relationships with intrinsic axons in the cat motor cortex. Somatosens Mot Res 2000;17:67–80. [PubMed: 10833086]

Porter LL, Sakamoto T, Asanuma H. Morphological and physiological identification of neurons in the cat motor cortex which receive direct input from the somatic sensory cortex. Exp Brain Res 1990;80:209–212. [PubMed: 2358029]

Reading SAJ, Dziorny AC, Peroutka LA, Schreiber M, Gourley LM, Yallapragada V, Rosenblatt A, Margolis RL, Pekar JJ, Pearlson GD, Aylward E, Brandt J, Bassett SS. Functional brain changes in presymptomatic Huntington's Disease. Annals of Neurology 2004;55:879–883. [PubMed: 15174024]

Santhakumar V, Soltesz I. Plasticity of interneuronal species diversity and parameter variance in neurological diseases. Trends Neurosci 2004;27:504–510. [PubMed: 15271499]

Shipp S. The importance of being agranular: a comparative account of visual and motor cortex. Philos Trans R Soc Lond B Biol Sci 2005;360:797–814. [PubMed: 15937013]

Starling AJ, Andre VM, Cepeda C, de Lima M, Chandler SH, Levine MS. Alterations in N-Methyl-D-Aspartate receptor sensitivity and magnesium blockade occur early in development in the R6/2 mouse model of Huntington's Disease. J Neurosci Res 2005;82:377–386. [PubMed: 16211559]

Strong TV, Tagle DA, Valdes JM, Elmer LW, Boehm K, Swaroop M, Kaatz KW, Collins FS, Albin RL. Widespread expression of the human and rat Huntington's disease gene in brain and nonneural tissues. Nat Genet 1993;5:259–265. [PubMed: 8275091]

The Huntington's Disease Collaborative Research Group. A novel gene containing a trinucleotide repeat that is expanded and unstable on Huntington's disease chromosomes. Cell 1993;72:971–983. [PubMed: 8458085]

Thiruvady DR, Georgiou-Karistianis N, Egan GF, Ray S, Sritharan A, Farrow M, Churchyard A, Chua P, Bradshaw JL, Brawn TL, Cunnington R. Functional connectivity of the prefrontal cortex in Huntington's disease. J Neurol Neurosurg Psychiatry 2007;78:127–133. [PubMed: 17028117]

Thomson AM, Bannister AP. Interlaminar connections in the neocortex. Cereb Cortex 2003;13:5–14. [PubMed: 12466210]

Truant R, Atwal R, Burtnik A. Hypothesis: Huntingtin may function in membrane association and vesicular trafficking. Biochem Cell Biol 2006;84:912–917. [PubMed: 17215878]

Usdin MT, Shelbourne PF, Myers RM, Madison DV. Impaired synaptic plasticity in mice carrying the Huntington's disease mutation. Hum Mol Genet 1999;8:839–846. [PubMed: 10196373]

Vonsattel JP, DiFiglia M. Huntington disease. J Neuropathol Exp Neurol 1998;57:369–384. [PubMed: 9596408]

Vonsattel JP, Myers RH, Stevens TJ, Ferrante RJ, Bird ED, Richardson EP Jr. Neuropathological classification of Huntington's disease. J Neuropathol Exp Neurol 1985;44:559–577. [PubMed: 2932539]

Williams SR, Mitchell SJ. Direct measurement of somatic voltage clamp errors in central neurons. Nature Neuroscience 2008;11:790–798.

Womelsdorf T, Fries P. The role of neuronal synchronization in selective attention. Curr Opin Neurobiol 2007;17:154–160. [PubMed: 17306527]

Zuccato C, Cattaneo E. Role of brain-derived neurotrophic factor in Huntington's disease. Prog Neurobiol 2007;81:294–330. [PubMed: 17379385]

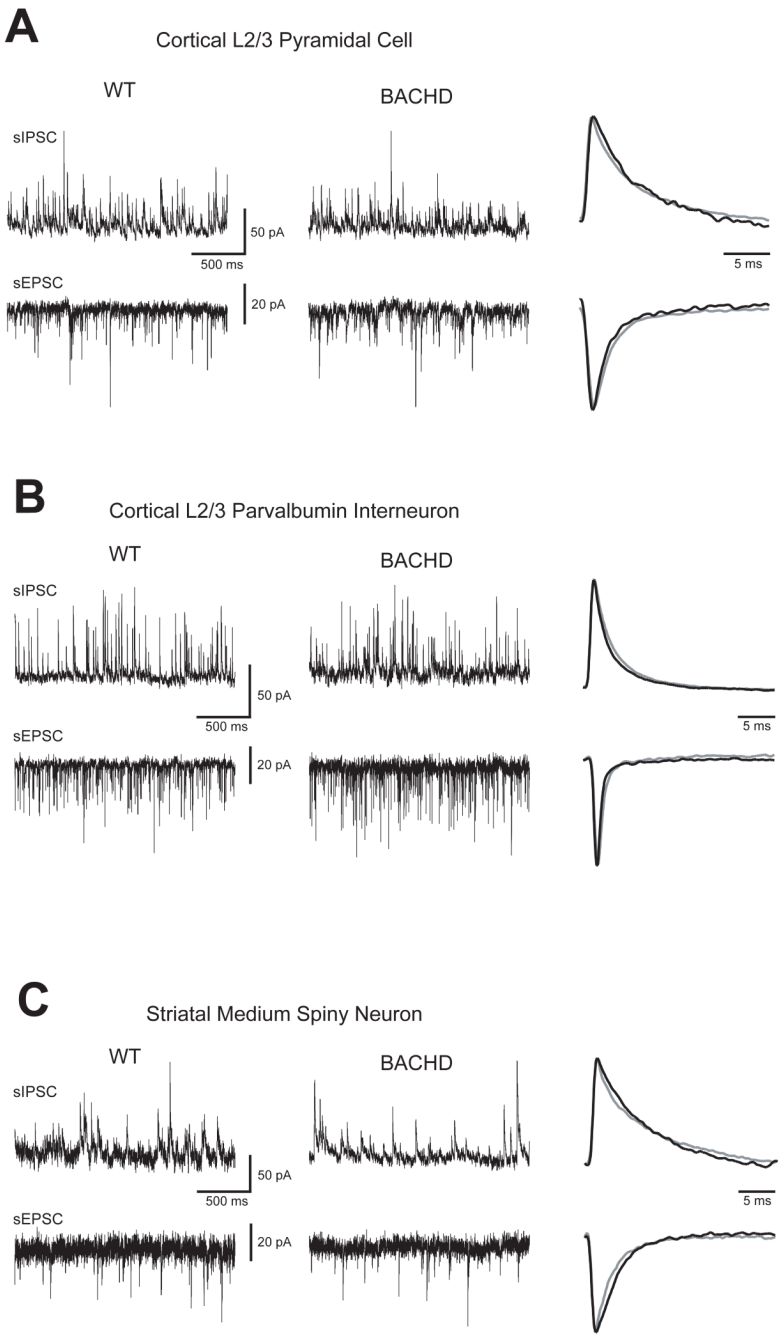

Figure 1. Spontaneous IPSC and EPSC are similar in individual cells of 3 month old WT and BACHD mice

Typical sIPSC (upward deflections) and sEPSC (downward deflections) recorded in the same cell from WT or BACHD mice for each group and the normalized average unitary currents (far right, WT=*grey*, BACHD=*black*): **A.** Raw traces recorded from visually identified primary motor cortex layer 2/3 pyramidal cells. **B.** Raw traces recorded from GFP-expressing primary motor cortex layer 2/3 parvalbumin interneurons. **C.** Raw traced recorded from visually identified striatal medium spiny neurons.

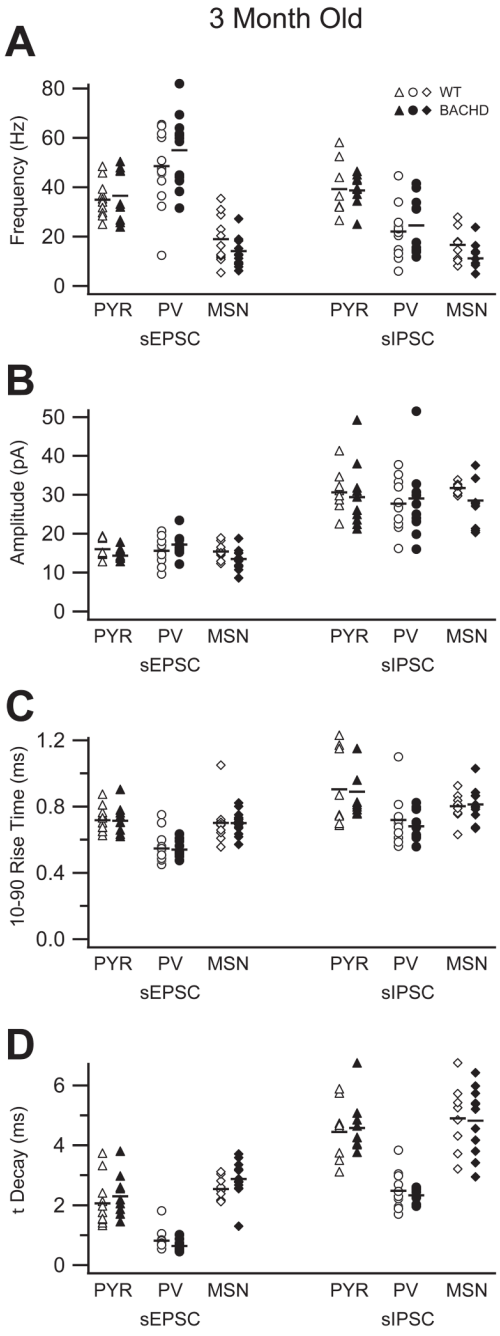

Figure 2. Group averages of spontaneous IPSC and EPSC show no differences between 3 month old WT and BACHD mice

No difference was observed in the frequency, amplitude, 10–90% rise time or decay time of sIPSC or sEPSC between BACHD (*black symbols*) and WT (*white symbols*) mice in either primary motor cortex layer 2/3 pyramidal cells (PYR, *triangles*), parvalbumin interneurons (PV, *circles*) or striatal medium spiny neurons (MSN, *diamonds*). In each plot symbols represent data from individually recorded cells and black bars indicate the group mean.

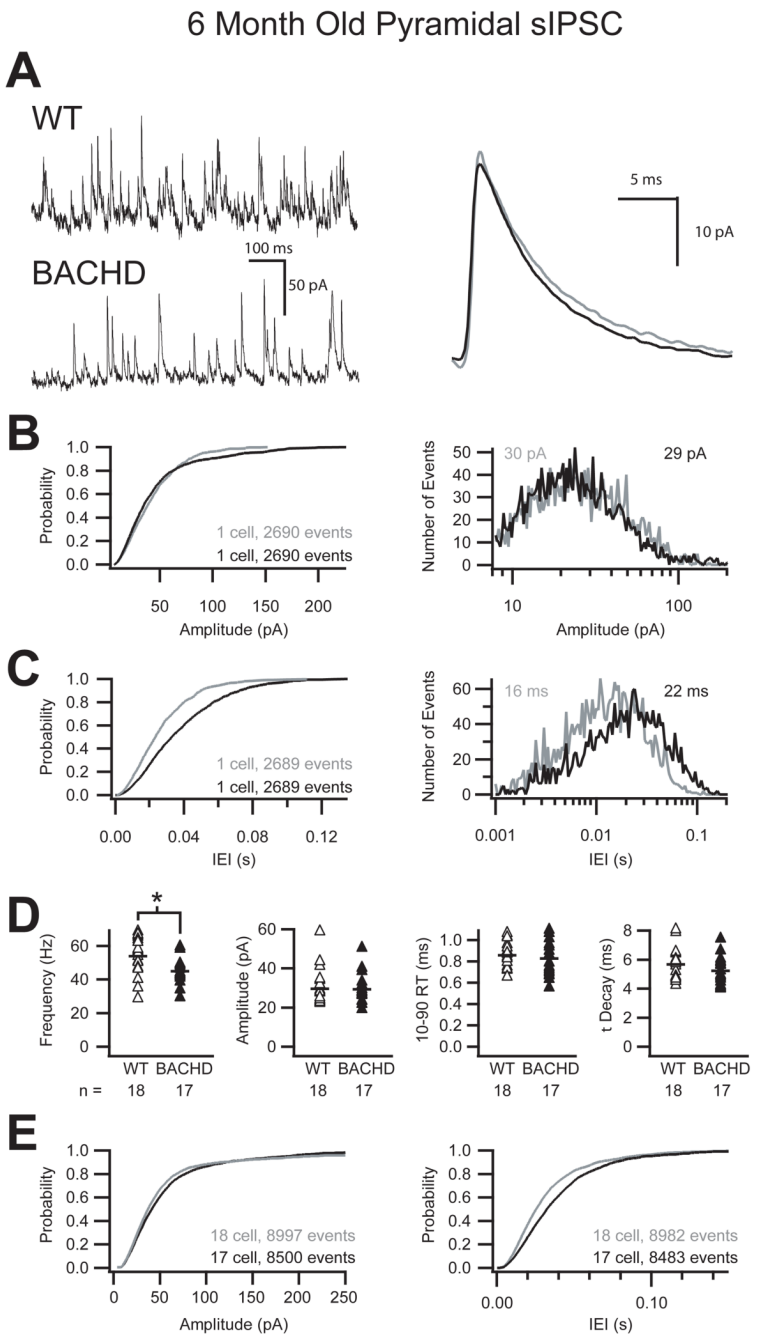

Figure 3. Reduced frequency of sIPSC onto pyramidal cells in 6 month old BACHD mice

A. Raw sIPSC recorded from a typical pyramidal cell from either WT or BACHD mice at 6 months of age demonstrating a reduction in the frequency of sIPSC in BACHD mice with no change in the average unitary current (right, WT=*grey*, BACHD=*black*). **B.** Cumulative probability and event distribution histogram of more than 2,600 sequential events illustrate no change in the amplitude of sIPSC between BACHD and WT mice. The mean for each distribution is indicated (WT=*grey*, BACHD=*black*). **C.** Cumulative probability and event distribution histogram of the same sequential events in B demonstrate a shift toward longer inter-event intervals (IEI) between sIPSC in BACHD mice compared to WT. **D.** Comparison of the average frequency, amplitude, 10–90% rise time and decay (τ) of sIPSC from all recorded

primary motor cortex layer 2/3 pyramidal cells (black bars indicate group averages, asterisk indicates significant difference, $p \leq 0.01$). **E.** Combined cumulative probabilities of sIPSC amplitude and frequency of more than 8,000 events from all cells illustrates the significant shift towards longer inter-event intervals (*right*) between sIPSC in BACHD mice compared to WT littermates with no change in the amplitudes of those events (*left*).

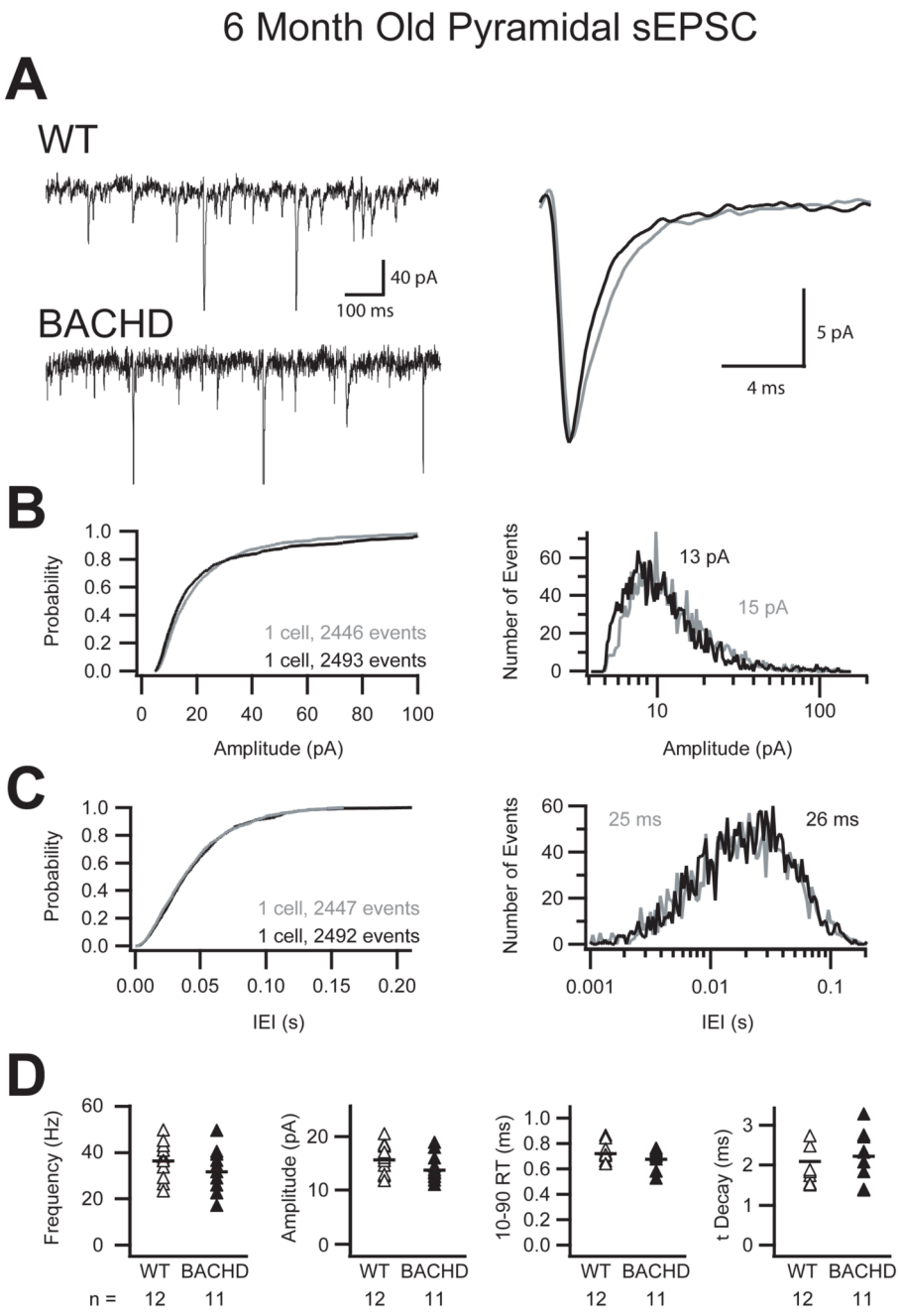

Figure 4. No change in sEPSC onto pyramidal cells in 6 month old BACHD mice

A. Raw sEPSC recorded from a typical pyramidal cell from either WT or BACHD mice at 6 months postnatal (right, WT=*grey*, BACHD=*black*). **B & C.** Cumulative probability and event distribution histogram of more than 2,400 sequential events illustrate no change in the amplitude or inter-event interval of sEPSC between BACHD and WT mice. Histogram means are indicated (WT=*grey*, BACHD=*black*). **D.** Comparison of the average frequency, amplitude, 10–90% rise time and decay (τ) of sEPSC from all recorded primary motor cortex layer 2/3 pyramidal cells illustrating no differences between WT and BACHD mice. Symbols represent data from individually recorded cells and black bars indicate the group mean.

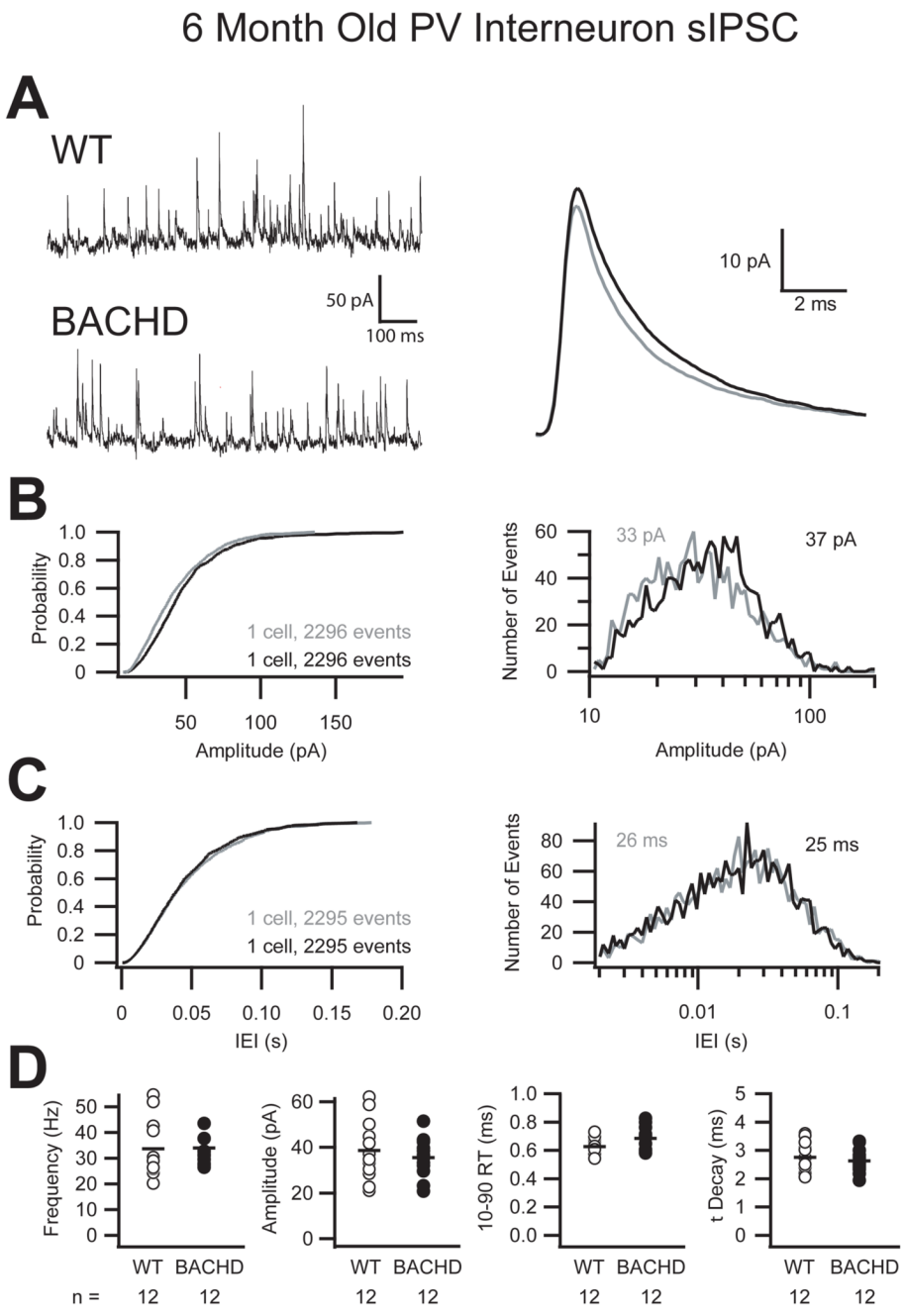

Figure 5. No change in sIPSC onto parvalbumin interneurons in 6 month old BACHD mice

A. Raw sEPSC recorded from a typical parvalbumin interneuron from either WT or BACHD mice at 6 months of age (right, WT=*grey*, BACHD=*black*). **B & C.** Cumulative probability and event distribution histogram of approximately 2,300 sequential events illustrate no change in the amplitude or inter-event interval of sIPSC between representative PV interneurons from BACHD and WT mice. Histogram means are indicated (WT=*grey*, BACHD=*black*). **D.** Comparison of the average frequency, amplitude, 10–90% rise time and decay (τ) of sIPSC from all recorded primary motor cortex layer 2/3 parvalbumin interneurons illustrating no differences between WT and BACHD mice. Symbols represent data from individually recorded cells and black bars indicate the group mean.

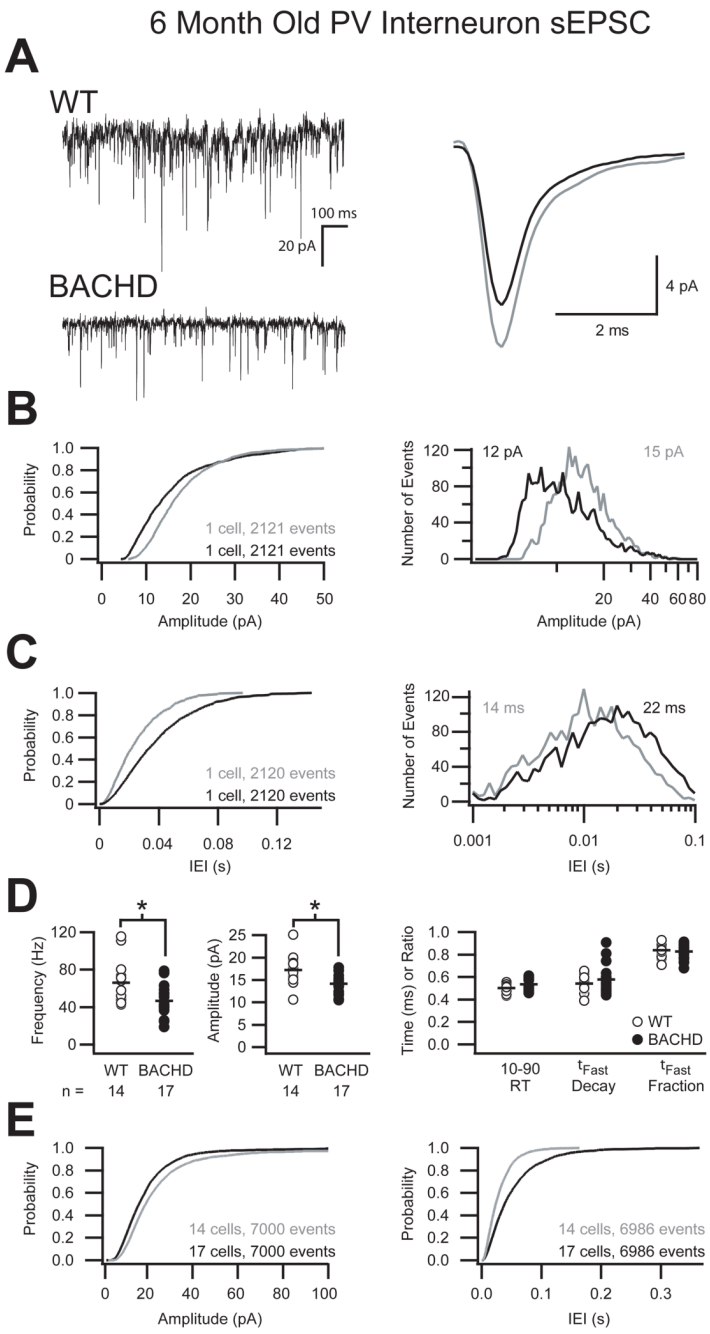

Figure 6. Reduced frequency and amplitude of sEPSC onto parvalbumin interneurons in 6 month old BACHD mice

A. Raw sEPSC recorded from typical parvalbumin interneurons from either WT or BACHD mice at 6 months postnatal demonstrating a reduction in the frequency and amplitude of sEPSC in BACHD mice with no change in the kinetics of the average unitary current (right, WT=*grey*, BACHD=*black*). **B.** Cumulative probability and event distribution histogram of more than 2,100 sequential events illustrates a shift towards smaller amplitude events in BACHD mice compared to WT. The mean for each distribution is indicated (WT=*grey*, BACHD=*black*). **C.** Cumulative probability and event distribution histogram of the same sequential events in B demonstrate a shift toward longer inter-event intervals (IEI) between

sEPSC in BACHD mice compared to WT. **D.** Comparison of the average frequency, amplitude, 10–90% rise time, fast decay (τ_{Fast}) and ratio of current decayed with τ_{Fast} of sEPSC from all recorded primary motor cortex layer 2/3 parvalbumin interneurons (black bars indicate group means, asterisk indicates significant difference, $p \leq 0.01$). **E.** Combined cumulative probabilities of sEPSC amplitude and frequency of 7,000 events from all cells illustrates the significant shift towards smaller amplitude events (*left*) and longer inter-event intervals (*right*) between sEPSC in BACHD mice compared to WT littermates.

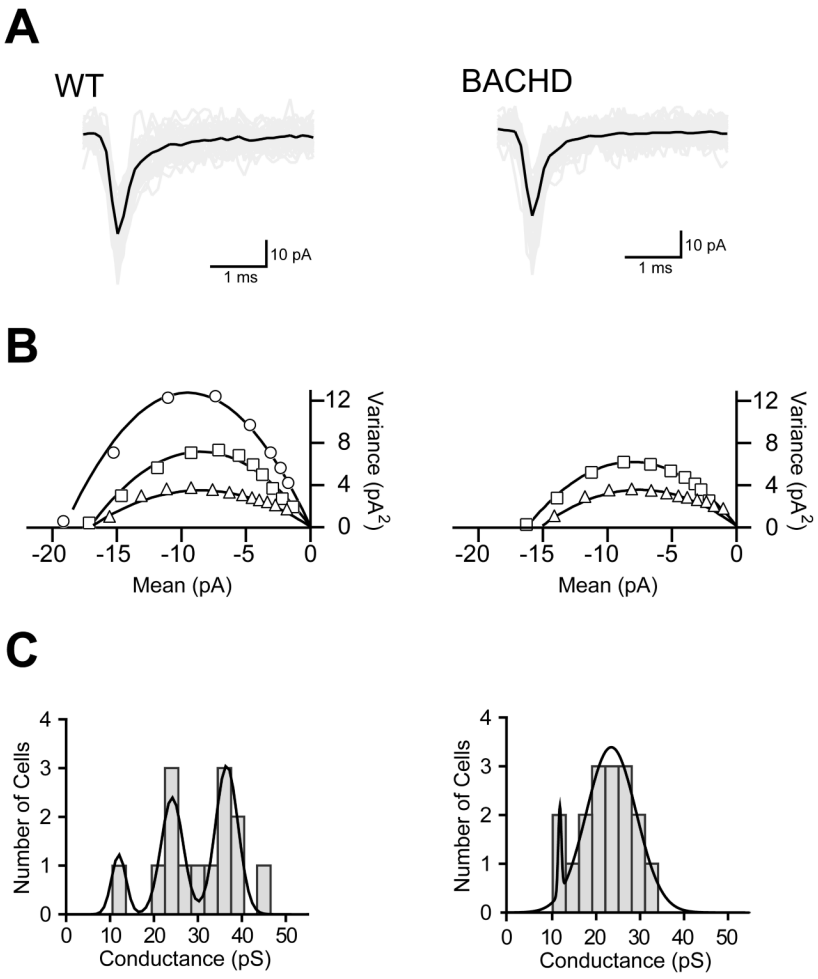

Figure 7. Non-stationary noise analysis of sEPSC onto parvalbumin interneurons in 6 month old BACHD mice

A Sample spontaneous events that were used to determine the average excitatory global single channel conductance of a given cell are displayed with the raw traces shown in grey and the average in black. **B**: Sample mean vs. variance plots and parabolic fits demonstrating the three different conductance states observed in WT PV interneurons and the two conductance states observed in BACHD PV interneurons. **C**: Histograms of the average excitatory global single channel conductance of each WT parvalbumin interneuron illustrating that the cells fall into three primary conductance states corresponding to the peaks of the triple Gaussian fit at 12.0 pS, 24.1 pS, and 36.6 pS; while the BACHD cells were better fit with two Gaussians centered at 12.1 pS and 23.9 pS.

Table 1

Synaptic and Passive Properties of Motor Cortex Layer 2/3 Pyramidal Cells, Parvalbumin Interneurons and Striatal Medium Spiny Neurons from 3 Month Old Mice.

		Pyramidal Cells		Parvalbumin Interneurons		Medium Spiny Neurons	
		WT	**BACHD**	**WT**	**BACHD**	**WT**	**BACHD**
EPSC	**Frequency (Hz)**	34.8 ± 7.4	36.4 ± 10.8	48.5 ± 15.6	54.9 ± 14.6	18.8 ± 9.7	13.9 ± 5.8
	Amplitude (pA)	16.0 ± 2.4	14.3 ± 1.6	15.5 ± 3.6	17.1 ± 2.7	15.3 ± 2.1	13.4 ± 2.5
	10–90 RT (ms)	0.72 ± 0.08	0.71 ± 0.09	0.55 ± 0.09	0.54 ± 0.05	0.70 ± 0.13	0.70 ± 0.07 #
	Decay (ms)	2.06 ± 0.82	2.30 ± 0.72	0.81 ± 0.34	0.64 ± 0.18 #	2.54 ± 0.36	2.87 ± 0.60
	I_{Mean} (pA/sec)	1.16 ± 0.33	0.99 ± 0.61	1.32 ± 0.40	1.60 ± 0.74 #	1.02 ± 0.23	0.78 ± 0.44 #
	n	10	9	13	12	11	14
IPSC	**Frequency (Hz)**	39.2 ± 10.9	38.6 ± 6.2	22.0 ± 10.4	24.4 ± 12.1	16.5 ± 7.0	11.0 ± 5.6
	Amplitude (pA)	30.5 ± 5.5	29.3 ± 8.5	27.6 ± 6.2	29.0 ± 9.8	31.7 ± 1.4	28.4 ± 5.8 #
	10–90 RT (ms)	0.90 ± 0.23	0.89 ± 0.19	0.72 ± 0.14	0.68 ± 0.09	0.80 ± 0.09	0.81 ± 0.10
	Decay (ms)	4.44 ± 1.00	4.57 ± 0.90	2.48 ± 0.62	2.33 ± 0.23 #	4.90 ± 1.14	4.82 ± 1.12
	I_{Mean} (pA/sec)	5.35 ± 2.54	5.62 ± 3.58	2.15 ± 2.22	1.89 ± 1.76	4.04 ± 1.27	2.94 ± 1.07
	n	8	10	12	9	8	11
Passive	**Input Resist. (MΩ)**	69.4 ± 28.9	76.2 ± 43.0	130.6 ± 58.6	112.1 ± 75.1	96.5 ± 63.9	104.6 ± 39.4
	τ(ms)	1.69 ± 0.45	1.89 ± 0.33	1.09 ± 0.21	1.25 ± 0.40 #	1.28 ± 0.17	1.47 ± 0.42 #
	Decay ratio	0.68 ± 0.05	0.70 ± 0.06	0.49 ± 0.17	0.38 ± 0.11	0.76 ± 0.07	0.79 ± 0.06
	N	12	10	13	12	12	16

# Indicates a significant difference in the variance between WT and BACHD within the cell type (F-test, $p \leq 0.05$)

Table 2

Synaptic and Passive Properties of Motor Cortex Layer 2/3 Pyramidal Cells and Parvalbumin Interneurons from 6 Month Old Mice.

		Pyramidal Cells		Parvalbumin Interneurons	
		WT	**BACHD**	**WT**	**BACHD**
EPSC	**Frequency (Hz)**	36.3 ± 8.1	31.7 ± 9.0	66.1 ± 23.5 ¤	46.6 ± 16.6 **
	Amplitude (pA)	15.7 ± 2.7	13.8 ± 2.5	17.2 ± 3.4	14.1 ± 2.2 **¤¤
	10–90 RT (ms)	0.72 ± 0.06	0.68 ± 0.07	0.50 ± 0.03	0.53 ± 0.06 *
	Decay (ms)	2.11 ± 0.63	2.24 ± 0.58	0.54 ± 0.08	0.57 ± 0.13
	I_{Mean} (pA/sec)	1.38 ± 0.54	0.75 ± 0.30 **‡	1.72 ± 0.90 ‡	0.92 ± 0.44 **#¤¤
	n	12	11	14	17
IPSC	**Frequency (Hz)**	54.0 ± 11.3 ¤¤	44.9 ± 7.5 **¤	33.5 ± 11.2	33.8 ± 8.2
	Amplitude (pA)	29.9 ± 9.6	29.6 ± 7.6	38.7 ± 13.2	35.5 ± 8.6
	10–90 RT (ms)	0.86 ± 0.12	0.82 ± 0.17	0.63 ± 0.06	0.68 ± 0.08
	Decay (ms)	5.64 ± 1.12	5.20 ± 0.97	2.75 ± 0.53	2.63 ± 0.42
	I_{Mean}(pA/sec)	10.62 ± 6.02 ¤¤‡	7.34 ± 3.29 *#	3.63 ± 2.07	4.02 ± 2.28
	n	18	17	12	12
Passive	**Input Resist. (MΩ)**	64.3 ± 22.3	71.2 ± 17.9	89.7 ± 38.4	102.1 ± 44.5
	τ(ms)	1.88 ± 0.5	1.86 ± 0.4	1.15 ± 0.3	1.21 ± 0.4
	Decay ratio	0.70 ± 0.08	0.72 ± 0.05	0.47 ± 0.09	0.54 ± 0.05 **
	n	23	20	19	17

** Indicates a significant difference between WT and BACHD within the cell type (Student's t-Test, $p \leq 0.01$)

* Indicates a significant difference between WT and BACHD within the cell type (Student's t-Test, $p \leq 0.05$)

# Indicates a significant difference in the variance between WT and BACHD within the cell type (F-test, $p \leq 0.05$)

¤¤ Indicates a significant difference between 3 and 6 month old animals within the cell type and genotype (Student's t-Test, $p \leq 0.01$)

¤ Indicates a significant difference between 3 and 6 month old animals within the cell type and genotype (Student's t-Test, $p \leq 0.05$)

‡ Indicates a significant difference in the variance between 3 and 6 month old animals within the cell type and genotype (F-test, $p \leq 0.05$)